January 7th, 2022

Star Formation Newsletter No.347 30-35

Shota Notsu (RIKEN)

-30: A cold accretion flow onto one component of a multiple protostellar system

-31: From Pebbles and Planetesimals to Planets and Dust: the Protoplanetary Disk--Debris Disk Connection

-32: Structure of IRAS 05168+3634 star-forming region

-33: Rebounding Cores to Build Star Cluster Multiple Populations

-34: Chemical environments of 6.7 GHz methanol maser sources

-35: Galactic Star Formation with NIKA2 (GASTON): Evidence of mass accretion onto dense clumps

-補足解説スライド: HCN/HNC比を用いたガス温度測定 (Hacar et al. 2020)

https://arxiv.org/abs/2111.04039v1

30

A cold accretion flow onto one component of a multiple protostellar system

Nadia M. Murillo, Ewine F. van Dishoeck, Alvaro Hacar, Daniel Harsono, Jes K. Jørgensen ★

Context: Gas accretion flows transport material from the cloud core onto the protostar. In multiple protostellar systems, it is not clear if the delivery mechanism is preferential or evenly distributed among the components. Aims: Gas accretion flows within IRAS16293 is explored out to 6000 AU. Methods: ALMA Band 3 observations of low-J transitions of HNC, cyanopolyynes (HC_3N, HC_5N), and N_2H^+ are used to probe the cloud core structure at 100 AU resolution. Additional Band 3 archival data provide low-J HCN and SiO lines. These data are compared with the corresponding higher-J lines from the PILS Band 7 data for excitation analysis. The HNC/HCN ratio is used as a temperature tracer. Results: The low-J transitions of HC_3N, HC_5N, HNC and N_2H^+ trace extended and elongated structures from 6000 AU down to 100 AU, without accompanying dust continuum emission. Two structures are identified: one traces a flow that is likely accreting toward the most luminous component of the system IRAS16293 A. Temperatures inferred from the HCN/HNC ratio suggest that the gas in this flow is cold, between 10 and 30 K. The other structure is part of an UV-irradiated cavity wall entrained by one of the outflows. The two outflows driven by IRAS16293 A present different molecular gas distributions. Conclusions: Accretion of cold gas is seen from 6000 AU scales onto IRAS16293 A, but not onto source B, indicates that cloud core material accretion is competitive due to feedback onto a dominant component in an embedded multiple protostellar system. The preferential delivery of material could explain the higher luminosity and multiplicity of source A compared to source B. The results of this work demonstrate that several different molecular species, and multiple transitions of each species, are needed to confirm and characterize accretion flows in protostellar cloud cores.

低質量原始星連星源 IRAS16293-2422 A&Bを、ALMA Band 3でr~100-6000 auの幅広い空間スケールにわたり観測。連星源へ落ち込む冷たいガスの流れや、Outflowの構造などを解析。

Source A とBの構造を比較し、降着流の存在とAの高い光度やbinarityを関連づけて議論。

ダスト連続波観測

赤&緑矢印：Source AからのOutflow

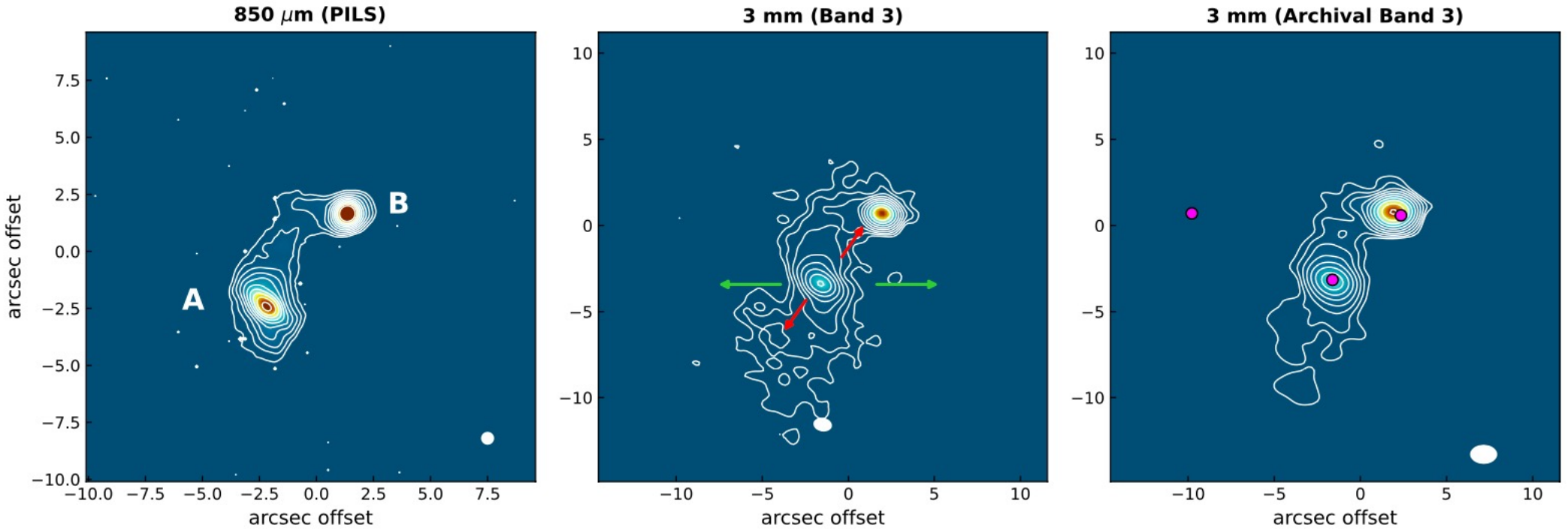

Source Aの方が明るい

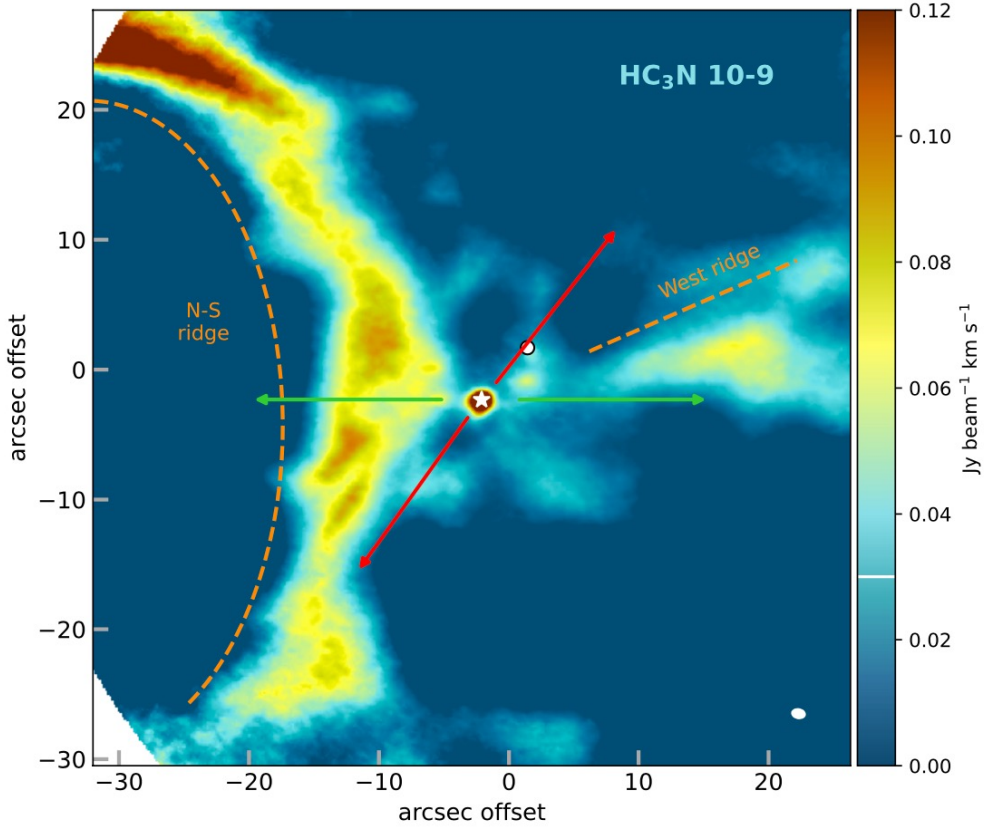

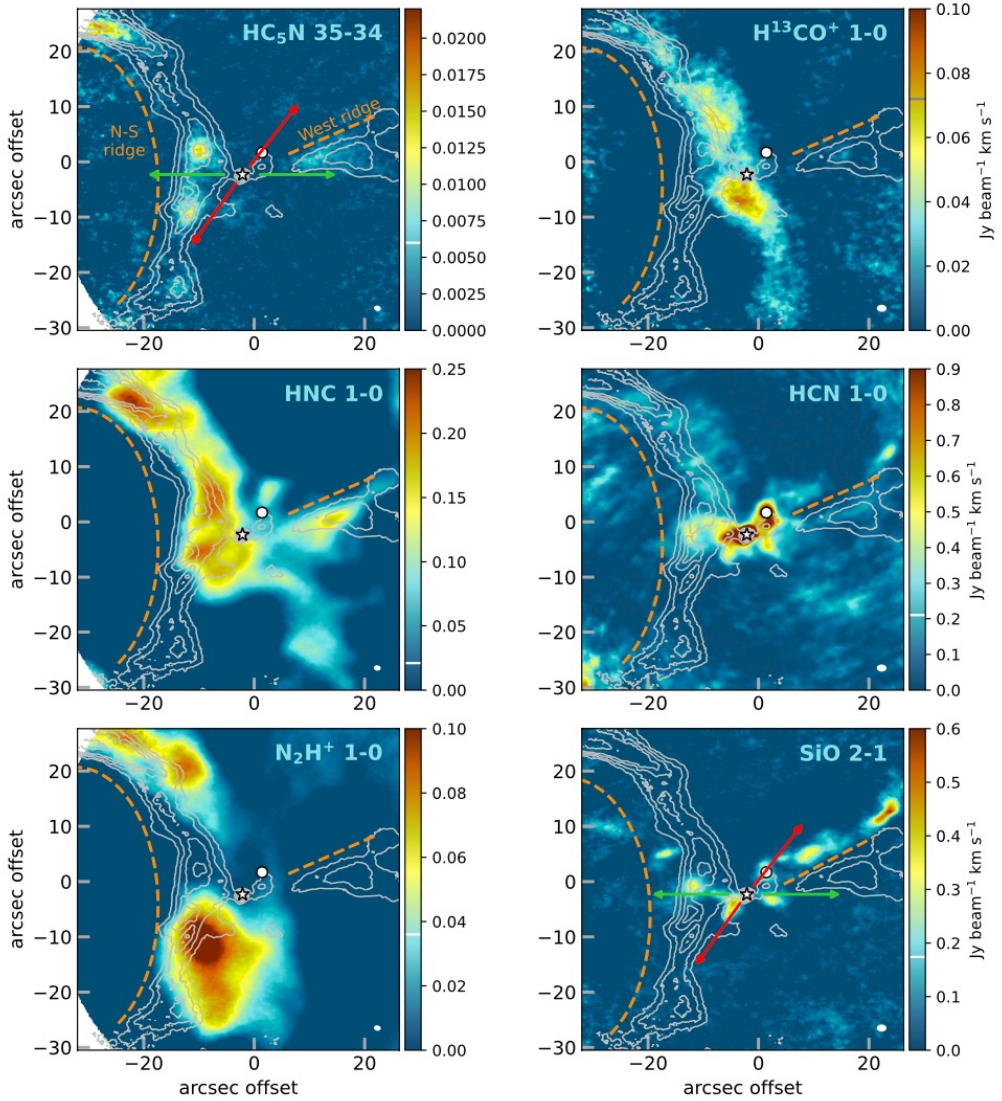

West ridge: outflow cavity wallに対応
N-S ridge: ダスト連続波では見えない構造 & 分子輝線毎に空間分布にoffsetあり

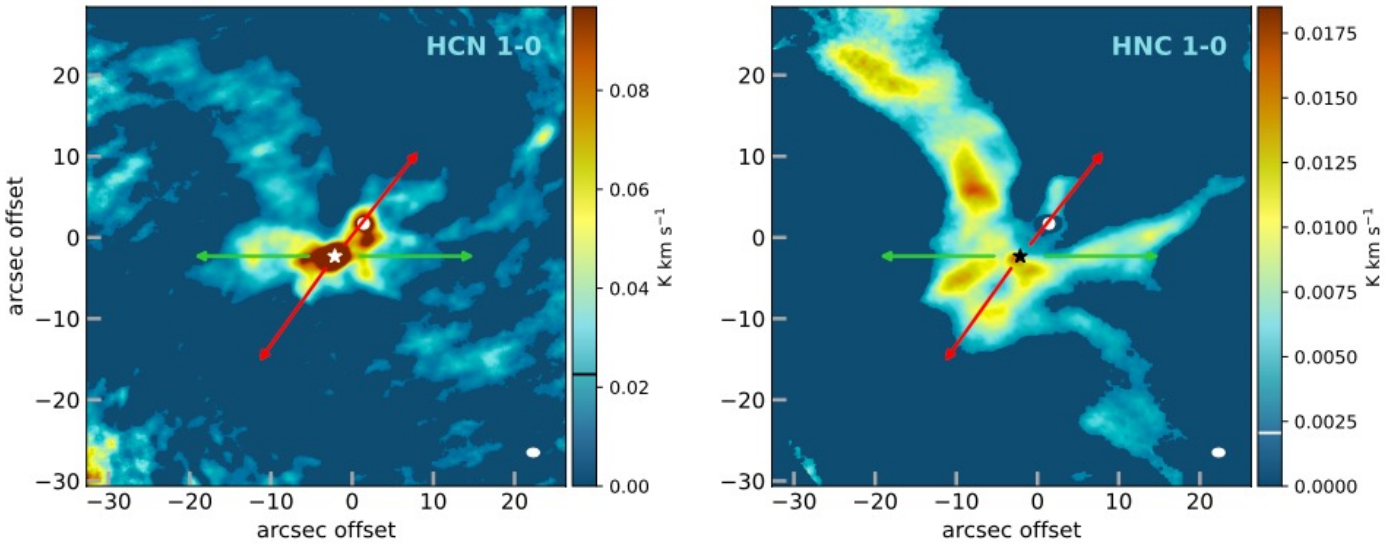

HCN/HNC 比 (J=1-0)：
分子雲等でのガス温度の指標 (Hacar, A., et al. 2020)

$$T_{\rm K} = 10 \times \frac{I({\rm HCN})}{I({\rm HNC})} \qquad if \quad 1 < \frac{I({\rm HCN})}{I({\rm HNC})} \leq 4$$

$$T_{\rm K} = 3 \times \left(\frac{I({\rm HCN})}{I({\rm HNC})} - 4 \right) + 40 \qquad if \quad \frac{I({\rm HCN})}{I({\rm HNC})} > 4.$$

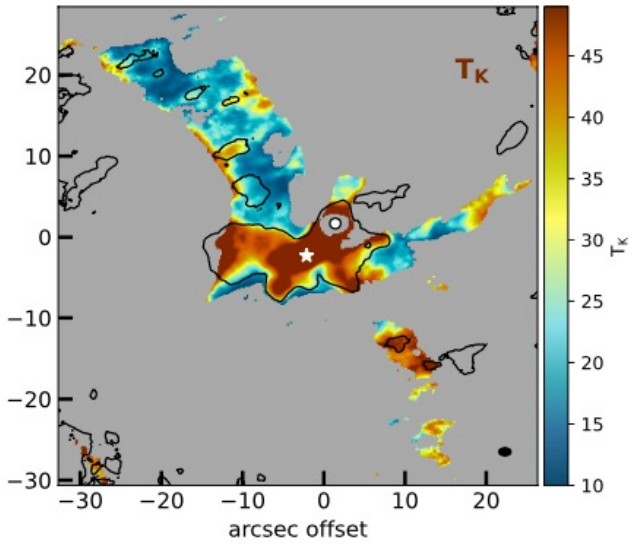

降着流は低温 (T_K<20 K)

https://arxiv.org/abs/2111.06406v1

31. **From Pebbles and Planetesimals to Planets and Dust: the Protoplanetary Disk–Debris Disk Connection**

Joan R. Najita, Scott J. Kenyon, Benjamin C. Bromley ★ The similar orbital distances and detection rates of debris disks and the prominent rings observed in protoplanetary disks suggest a potential connection between these structures. We explore this connection with new calculations that follow the evolution of rings of pebbles and planetesimals as they grow into planets and generate dusty debris. Depending on the initial solid mass and planetesimal formation efficiency, the calculations predict diverse outcomes for the resulting planet masses and accompanying debris signature. When compared with debris disk incidence rates as a function of luminosity and time, the model results indicate that the known population of bright cold debris disks can be explained by rings of solids with the (high) initial masses inferred for protoplanetary disk rings and modest planetesimal formation efficiencies that are consistent with current theories of planetesimal formation. These results support the possibility that large protoplanetary disk rings evolve into the known cold debris disks. The inferred strong evolutionary connection between protoplanetary disks with large rings and mature stars with cold debris disks implies that the remaining majority population of low-mass stars with compact protoplanetary disks leave behind only modest masses of residual solids at large radii and evolve primarily into mature stars without detectable debris beyond 30 au. The approach outlined here illustrates how combining observations with detailed evolutionary models of solids strongly constrains the global evolution of disk solids and underlying physical parameters such as the efficiency of planetesimal formation and the possible existence of invisible reservoirs of solids in protoplanetary disks.

原始惑星系円盤のリング構造とデブリ円盤の構造の関係を探るために、
ペブル&微惑星リングの進化を計算

円盤リングの初期質量や微惑星形成率などがパラメータ。依存性を調べた。
→観測される明るいデブリ円盤を再現するために必要な円盤リング初期質量などを議論

https://arxiv.org/abs/2111.02906v1

32. Structure of IRAS 05168+3634 star-forming region

E. H. Nikoghosyan, N. M. Azatyan, D. H. Andreasyan, D. S. Baghdasaryan
★ This study aims to determine the main physical parameters (N(H2) hydrogen column density and Td dust temperature) of the Interstellar medium, and their distribution in the extended star-forming region, which includes IRAS 05156+3643, 05162+3639, 05168+3634, 05177+3636, and 05184+3635 sources. We also provide a comparative analysis of the properties of the Interstellar medium and young stellar objects. Analysis of the results revealed that Interstellar medium forms relativity dense condensations around IRAS sources, which are interconnected by a filament structure. In general, in sub-regions Td varies from 11 to 24 K, and N(H2) - from 1.0 to 4.0 x 10^{23} cm^{-2}. The masses of the ISM vary from 1.7 x 10^4 to 2.1 x 10^5 Msol. All BGPSv2 objects identified in this star-forming region are located at the N(H2) maximum. The direction of the outflows, which were found in two sub-regions, IRAS 05168+3634 and 05184+3635, correlates well with the isodenses direction. The sub-regions with the highest N(H2) and Interstellar medium mass have the largest percentage of young stellar objects with Class I evolutionary stage. The wide spread of the evolutionary ages of stars in all sub-regions (from 10^5 to 10^7 years) suggests that the process of star formation in the considered region is sequential. In those sub-regions where the mass of the initial, parent molecular cloud is larger, this process is likely to proceed more actively. On the Gaia EDR3 database, it can be assumed that all sub-regions are embedded in the single molecular cloud and belong to the same star-forming region, which is located at a distance of about 1.9 kpc.

IRAS 05168+3634を含む星形成領域をHerschel等で観測し、
ダスト温度T_dや水素分子柱密度N_{H2}などの物理量を算出。
T_d とN_{H2}はHerschelデータから以下の指揮を使って算出。

$$S_\nu = B_\nu(\nu, T_d)\Omega(1 - e^{-\tau(\nu)}), \quad (1)$$

with

$$\tau(\nu) = \mu_{H_2} m_H k_\nu N(H_2), \quad (2)$$

$$M_{clump} = \mu_{H_2} m_H Area_{pix} \sum N(H_2), \quad (4)$$

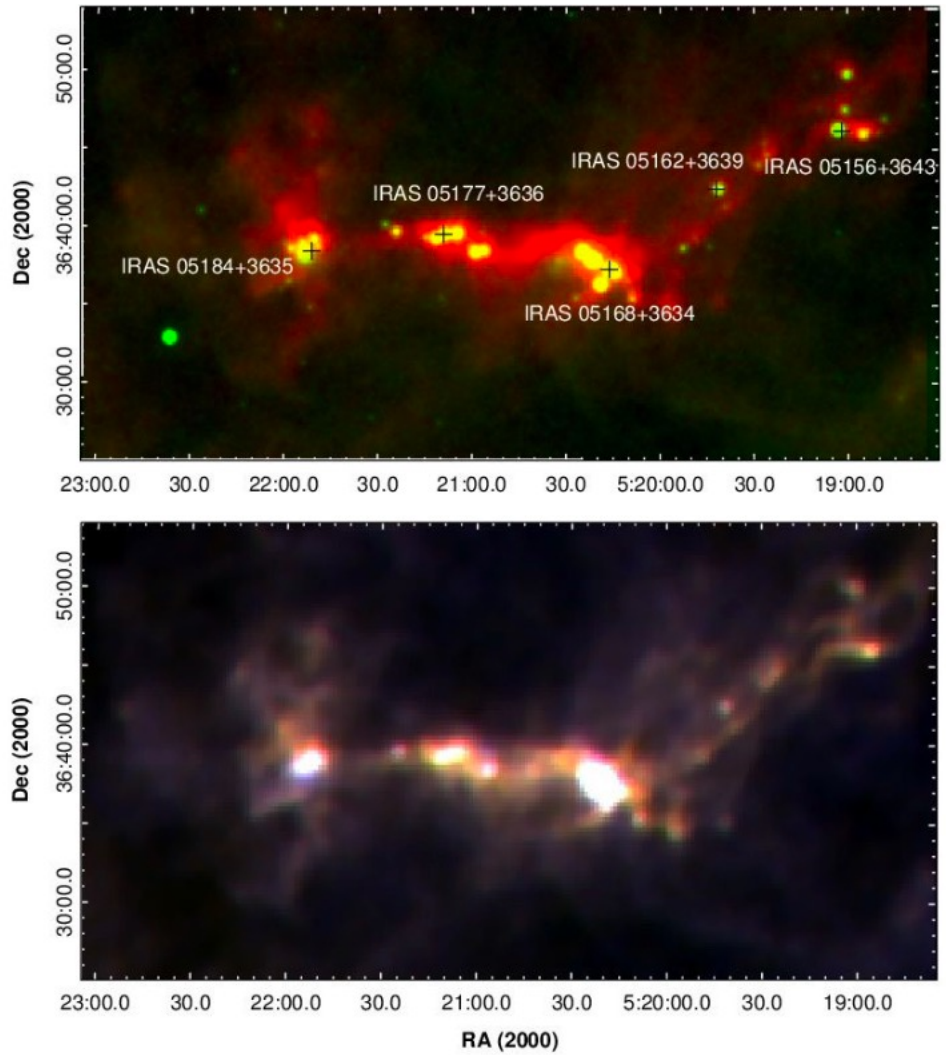

Fig. 1 Colour-composite images of IRAS 05168+3634 star-forming region. *Top panel*: W4 22 μm (green) and *Herschel* 500 μm (red), *bottom panel*: *Herschel* 160 μm (blue), 350 μm (green), and 500 μm (red). The positions of IRAS sources are marked by black crosses.

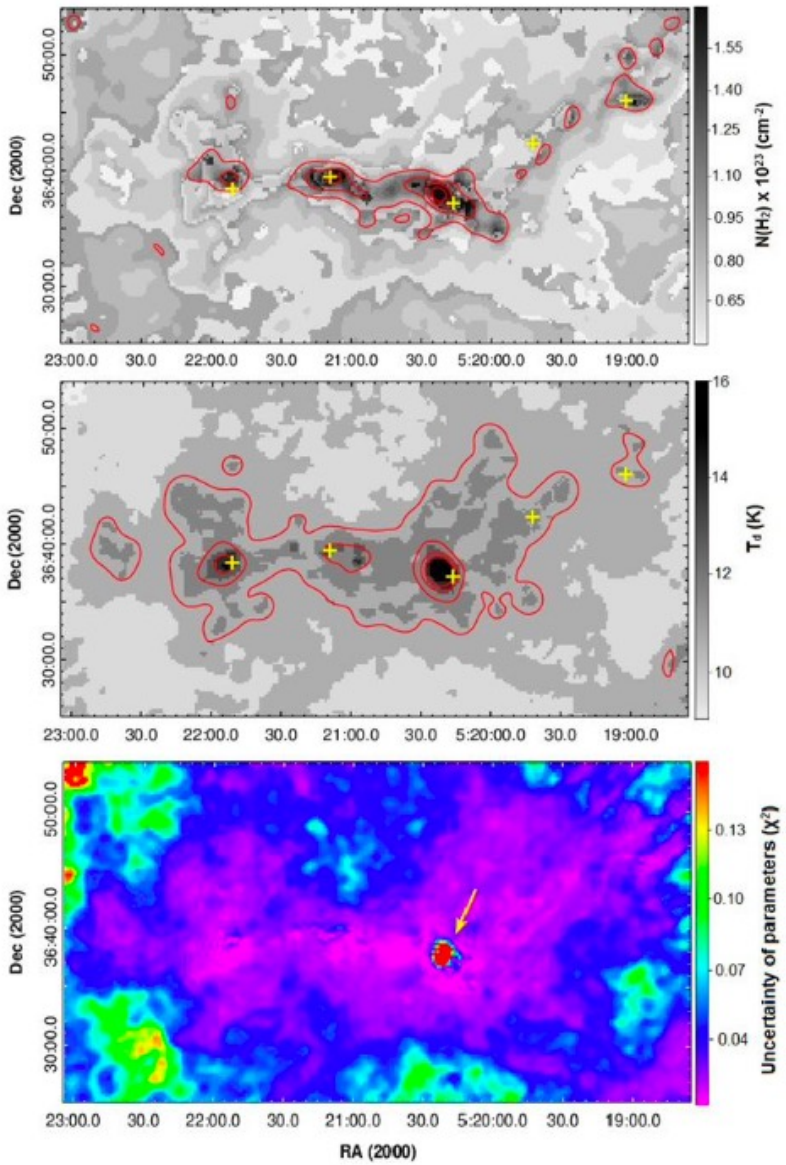

黄色十字が星形成領域の位置

矢印がIRAS 05168+3634

https://arxiv.org/abs/2110.14470v1

33. Rebounding Cores to Build Star Cluster Multiple Populations

G. Parmentier, A. Pasquali ★ We present a novel approach to the riddle of star cluster multiple populations. Stars form from molecular cores. But not all cores form stars. Following their initial compression, such 'failed' cores re-expand, rather than collapsing. We propose that their formation and subsequent dispersal regulate the gas density of cluster-forming clumps and, therefore, their core and star formation rates. Clumps for which failed cores are the dominant core type experience star formation histories with peaks and troughs. In contrast, too few failed cores results in smoothly decreasing star formation rates. We identify three main parameters shaping the star formation history of a clump: the star and core formation efficiencies per free-fall time, and the time-scale on which failed cores return to the clump gas. The clump mass acts as a scaling factor. We use our model to constrain the density and mass of the Orion Nebula Cluster progenitor clump, and to caution that the star formation histories of starburst clusters may contain close-by peaks concealed by stellar age uncertainties. Our model generates a great variety of star formation histories. Intriguingly, the chromosome maps and O-Na anti-correlations of old globular clusters also present diverse morphologies. This prompts us to discuss our model in the context of globular cluster multiple stellar populations. More massive globular clusters exhibit stronger multiple stellar population patterns, which our model can explain if the formation of the polluting stars requires a given stellar mass threshold.

星団の進化&分布の多様性に対し、星になれなかったコア('failed' cores)の存在がどう影響するかを考慮した研究。
Failed coreが拡散しガス密度に影響を与える事で、その後の星団内でのコア成長&星形成に影響を与えるとのこと。

https://arxiv.org/abs/2111.02074v2

34. Chemical environments of 6.7 GHz methanol maser sources

Sonu Tabitha Paulson, Jagadheep D. Pandian ★

6.7 GHz methanol masers are the brightest of class II methanol masers that are regarded as excellent signposts in the formation of young massive stars. We present here a molecular line study of 68 6.7 GHz methanol maser hosts chosen from the MMB catalogue, that have MALT90 data available. We performed (1) pixel-by-pixel study of 9 methanol maser sources that have high signal-to-noise ratio and (2) statistical study taking into account the entire 68 sources. We estimated the molecular column densities and abundances of N_2H^+(1-0), HCO^+(1-0), HCN(1-0) and HNC(1-0) lines. The derived abundances are found to be in congruence with the typical values found towards high mass star forming regions. We derived the column density and abundance ratios between these molecular species as an attempt to unveil the evolutionary stage of methanol maser sources. We found the column density and abundance ratio of HCN to HNC to increase and that of N_2H^+ to HCO^+ to decline with source evolution, as suggested by the chemical models. The HCN/HNC, N_2H^+/HCO^+, HNC/HCO^+ and N_2H^+/HNC ratios of the methanol maser sources are consistent with them being at a later evolutionary state than quiescent phase and possibly protostellar phase, but at an earlier stage than HII regions and PDRs.

6.7 GHz メタノールメーザー：大質量星形成場所の良い指標

今回の研究: 68個の6.7GHz メタノールメーザー源に対し、分子輝線観測を実施 (MALT90 Survey)
分子組成分布や柱密度分布から、進化段階などを議論。
HNC/HCN比を用いた温度測定も。

Transition	Frequency (MHz)	Tracer
HCO^+(1–0)	89188.526	Density; Kinematics
$H^{13}CO^+$(1–0)	86754.330	Optical depth, Column density, V_{LSR}
N_2H^+(1–0)	93173.772	Density, chemically robust
HCN (1–0)	88631.847	Density
HNC(1–0)	90663.572	Density; Cold chemistry
^{13}CS (2–1)	92494.303	Optical depth, Column density, V_{LSR}
CH_3CN 5(0)–4(0)	91987.086	Hot core
HC_3N (10–9)	90978.989	Hot core
$^{13}C^34S$ (2–1)	90926.036	Optical depth, Column density, V_{LSR}
$HC^{13}CCN$ (10–9)	90593.059	Hot core
HNCO 4(1,3)–3(1,2)	88239.027	Hot core
HNCO 4(0,4)–3(0,3)	87925.238	Hot core
C_2H (1–0) 3/2–1/2	87316.925	Photodissociation region
$HN^{13}C$ (1–0)	87090.859	Optical depth, Column density, V_{LSR}
SiO (1–0)	86847.010	Shock/outflow

上図：9個のメーザー源に対しpixel-by-pixel解析
下図：68個のメーザー源全てに対しての統計的解析

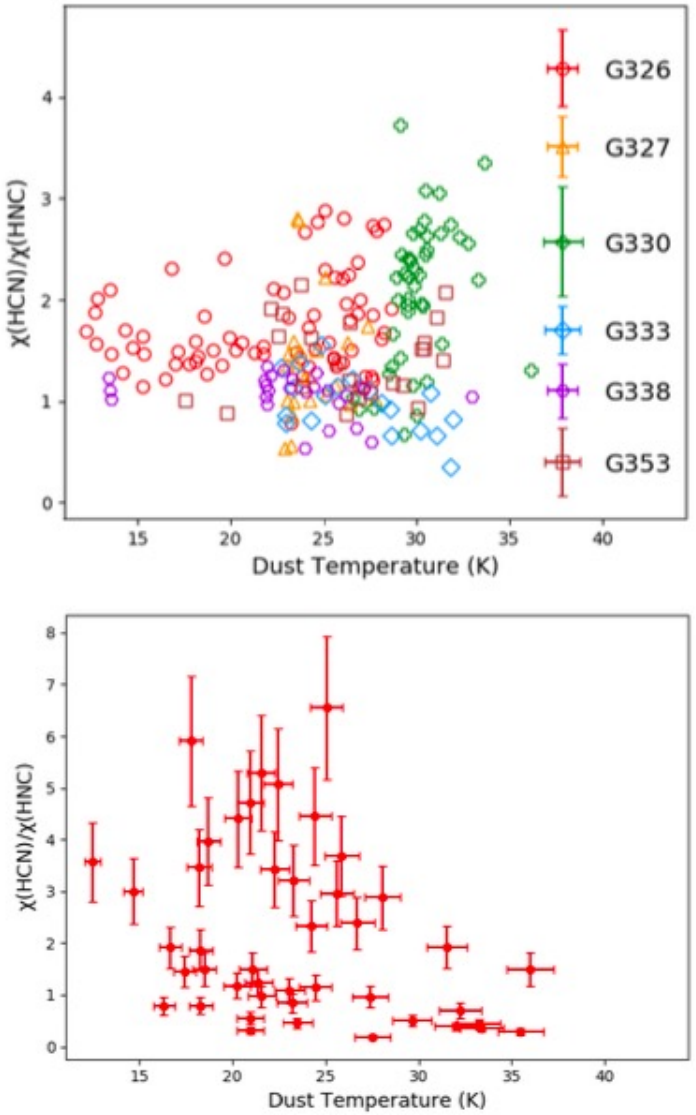

Figure 7. X(HNC)/X(HCN) vs dust temperature. The top panel (a) shows the plots for pixel-by-pixel study whereas the bottom panel (b) shows the results for statistical study.

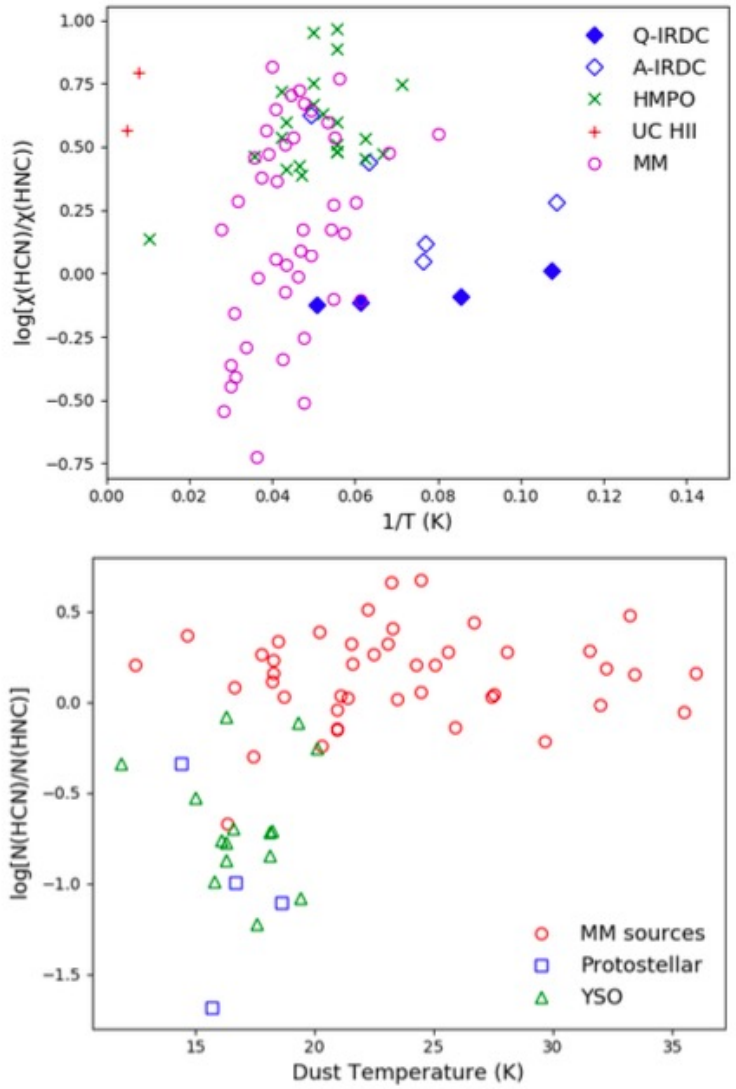

Figure 12. MM sources over plotted on results obtained by previous studies. The top panel shows the HCN/HNC ratios derived by Jin et al. (2015) and the bottom panel shows that of Saral et al. (2018).

メタノールメーザー源(MM)
：温度がより高い
→進化がより進んでいる？

https://arxiv.org/abs/2111.01668v3

35. Galactic Star Formation with NIKA2 (GASTON): Evidence of mass accretion onto dense clumps

GASTON collaboration A. J. Rigby et al. ★ High-mass stars ($m_* \gtrsim 8\,M_\odot$) play a crucial role in the evolution of galaxies, and so it is imperative that we understand how they are formed. We have used the New IRAM KIDs Array 2 (NIKA2) camera on the Institut de Radio Astronomie Millimétrique (IRAM) 30-m telescope to conduct high-sensitivity continuum mapping of ~ 2 deg^2 of the Galactic plane (GP) as part of the Galactic Star Formation with NIKA2 (GASTON) large program. We have identified a total of 1467 clumps within our deep 1.15 mm continuum maps and, by using overlapping continuum, molecular line, and maser parallax data, we have determined their distances and physical properties. By placing them upon an approximate evolutionary sequence based upon 8 μm *Spitzer* imaging, we find evidence that the most massive dense clumps accrete material from their surrounding environment during their early evolution, before dispersing as star formation advances, supporting clump-fed models of high-mass star formation.

IRAM 30m のNIKA2 cameraを使っての銀河面方向の連続波 mapping
1467個のclumpを同定し、周辺環境との相関などを議論

以下、時間が余った時のための補足解説スライド

HCN/HNC比を用いたガス温度測定 (Hacar et al. 2020)

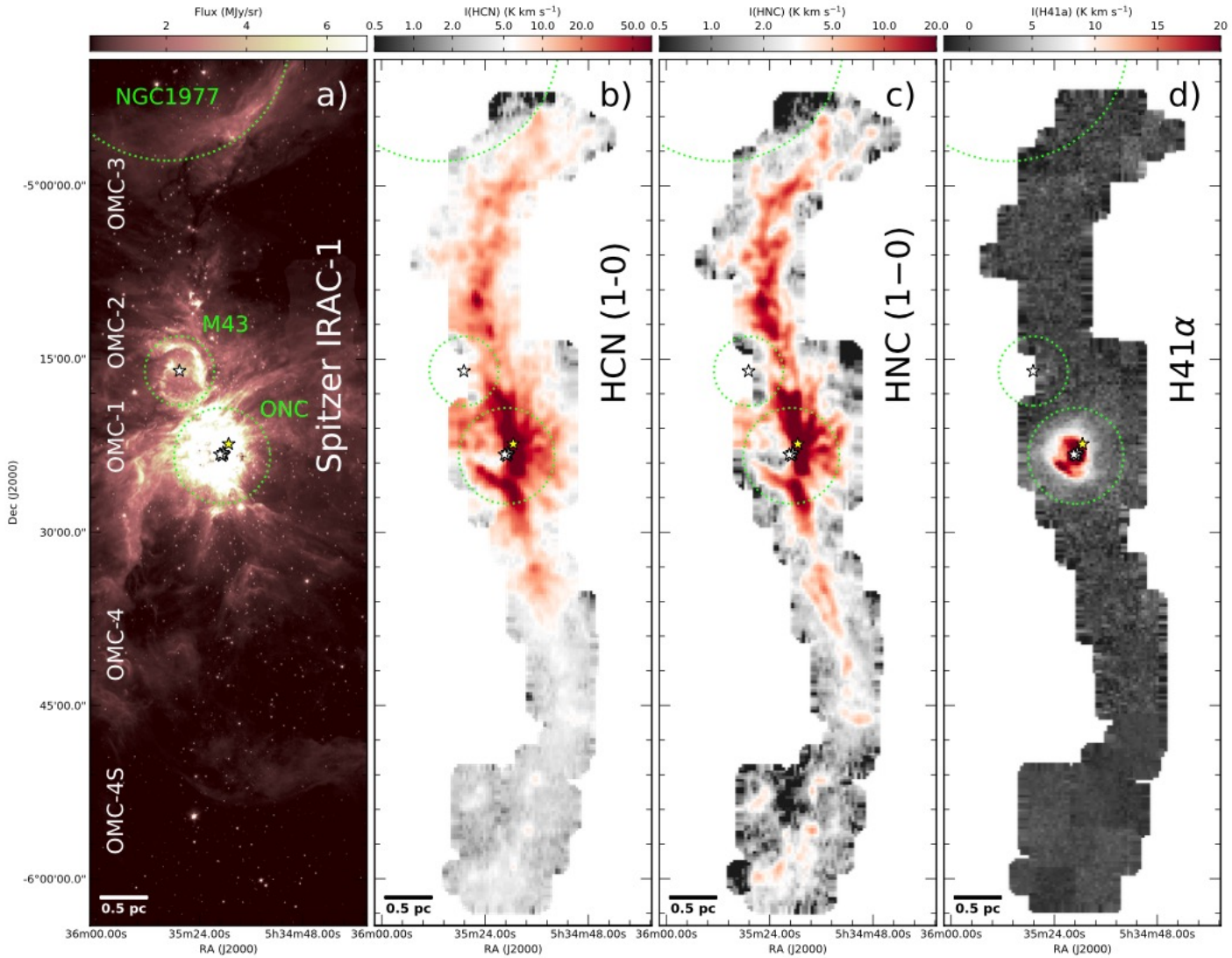
Flux (MJy/sr)
2
4
6
I(HCN) (K km s−1)
0.5
1.0
2.0
5.0
10.0
20.0
50.0
I(HNC) (K km s−1)
0.5
1.0
2.0
5.0
10.0
20.0
I(H41a) (K km s−1)
0
5
10
15
20
a)
b)
c)
d)
NGC1977
OMC-3
OMC-2
OMC-1
OMC-4
OMC-4S
M43
ONC
Spitzer IRAC-1
HCN (1-0)
HNC (1−0)
H41α
0.5 pc
-5°00'00.0"
15'00.0"
30'00.0"
45'00.0"
-6°00'00.0"
Dec (J2000)
36m00.00s
35m24.00s
5h34m48.00s
RA (J2000)

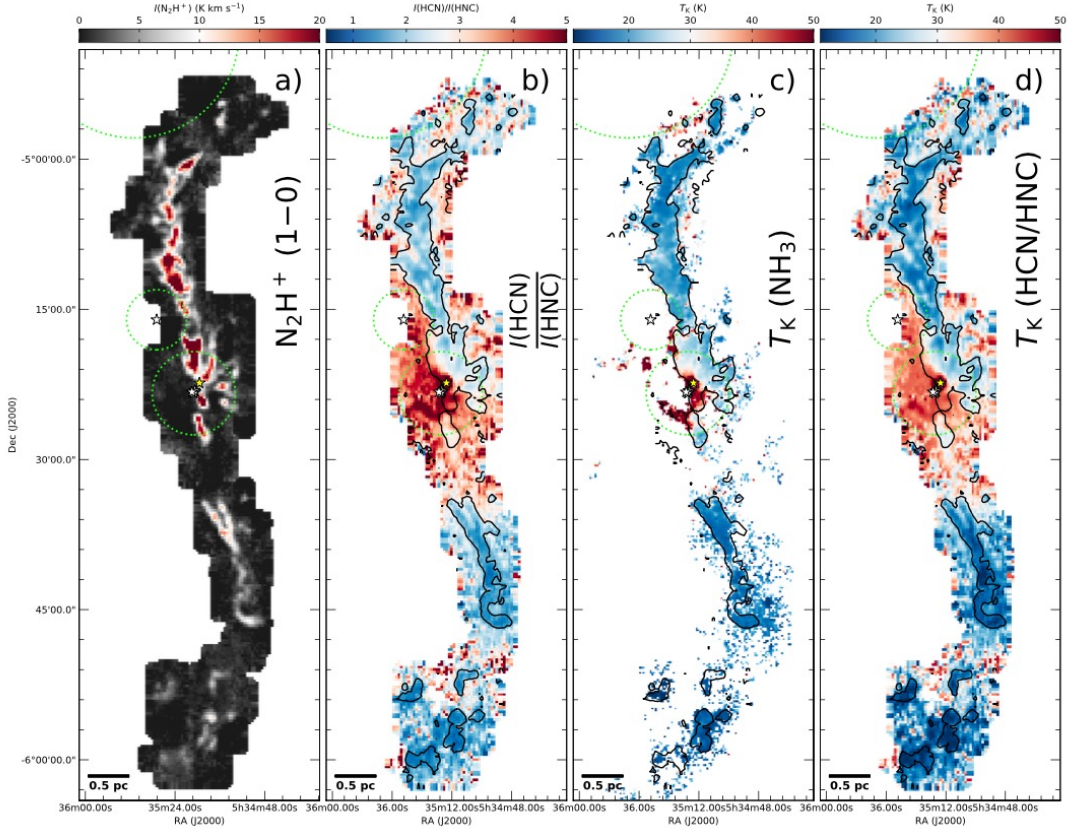

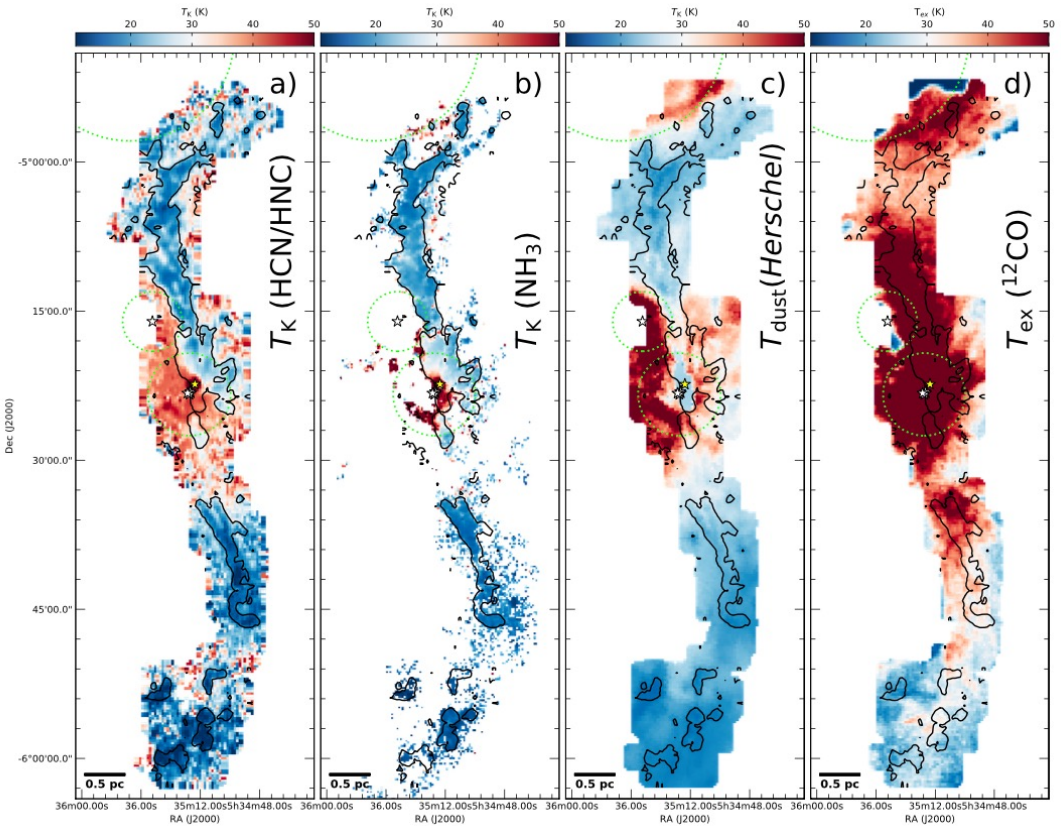

他の温度決定方法 (T_{dust}, T_K (NH_3), T_{ex} (^{12}CO)など) との比較

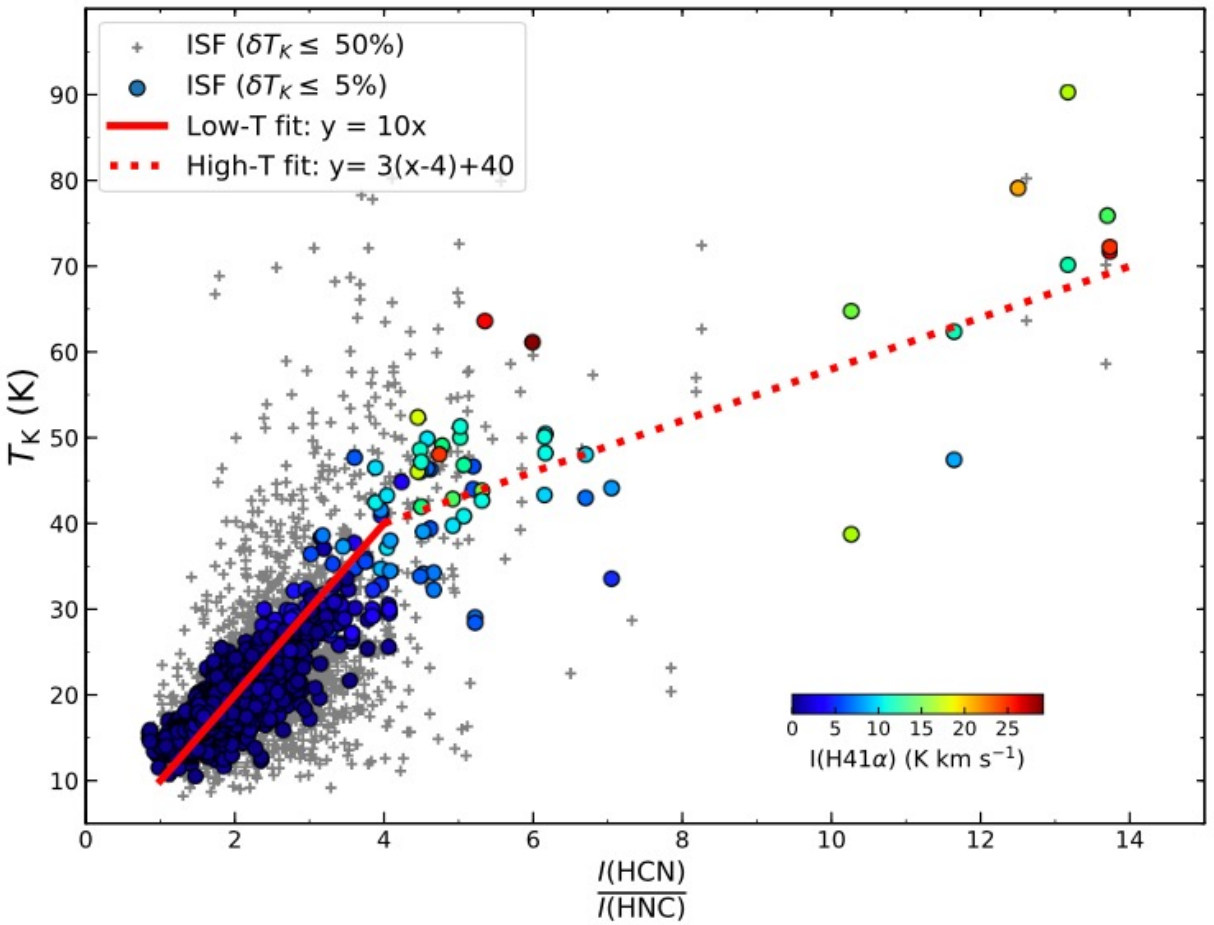

$$T_{\rm K}[{\rm K}] = 10 \times \left[\frac{I({\rm HCN})}{I({\rm HNC})}\right] \quad \text{if} \quad \left(\frac{I({\rm HCN})}{I({\rm HNC})}\right) \leq 4, \tag{3}$$

and

$$T_{\rm K}[{\rm K}] = 3 \times \left[\frac{I({\rm HCN})}{I({\rm HNC})} - 4\right] + 40 \quad \text{if} \quad \left(\frac{I({\rm HCN})}{I({\rm HNC})}\right) > 4. \tag{4}$$

左図のfitting式

上図のT_K: NH3から算出

概ねT_K~15~40 Kで良いfitting式

$$\mathrm{HNC + H \rightarrow HCN + H} \quad (1)$$

and

$$\mathrm{HNC + O \rightarrow NH + CO} \quad (2)$$